A Proposal for Diesel Spray Model Using a TAB Breakup Model and Discrete Vortex Method

Jeong-Kuk Yeom*
Mechanical and Aerospace Engineering Department, Graduate School of Seoul National University, Seoul 151-742, Korea
Myung-Jun Lee
Automotive Engineering Department, Yang-san College, Korea
Sung-Sik Chung, Jong-Yul Ha
Mechanical Engineering Department, Dong-A University, Korea
Jiro Senda, Hajime Fujimoto
Department of Mechanical Engineering, Doshisha University, Kyotanabe, Kyoto, Japan

A hybrid model consisting of a modified TAB (Taylor Analogy Breakup) model and DVM (Discrete Vortex Method) is proposed for numerical analysis of the evaporating spray phenomena in diesel engines. The simulation process of the hybrid model is divided into three steps. First, the droplet breakup of injected fuel is analyzed by using the modified TAB model. Second, spray evaporation is calculated based on the theory of Siebers' liquid length. The liquid length analysis of injected fuel is used to integrate the modified TAB model and DVM. Lastly, both ambient gas flow and inner vortex flow of injected fuel are analyzed by using DVM. An experiment with an evaporative free spray at the early stage of its injection was conducted under in-cylinder like conditions to examine an accuracy of the present hybrid model. The calculated results of the gas jet flow by DVM agree well with the experimental results. The calculated and experimental results all confirm that the ambient gas flow dominates the downstream diesel spray flow.

Key Words : Diesel Spray, Breakup Model, Hybrid Model, Vortex, Laser-Induced Fluorescence Technique

1. Introduction

Simple models were suggested for spray structure and spray combustion, in various simulation schemes, such as KIVA (KIVA-II, KIVA-3, and KIVA-3V) (Amsden, et al., 1985, 1989, 1993, 1997) and STAR-CD (Ahmadi-Befrui et al., 1996). In our study, models were developed to describe the breakup and diffusion process of a diesel impinging and free spray (Senda et al., 1994, 1997; Dan et al., 1997). However, these models could not accurately reproduce the macro characteristics of an injected spray, such as the spray tip penetration and the inner structure of an evaporating diesel spray. Therefore, we propose a hybrid model, which consists of the modified TAB (Taylor Analogy Breakup) model (O'Rourke, 1987) and DVM (Discrete Vortex Method) (Yamane et al., 1994), to numerically analyze the development of an actual spray. The TAB model was modified by simultaneously tuning the χ-squared distribution function with variation in the degree of freedom, Φ, and the ratio of the particle's distortion energy to its total energy, K, in the TAB model of a non-evapora-

* Corresponding Author,
E-mail : yjksnu@yahoo.co.kr
TEL : +82-2-880-8363; **FAX** : +82-2-874-2001
Mechanical and Aerospace Engineering Department, Graduate School of Seoul National University, Seoul 151-742, Korea. (Manuscript **Received** May 8, 2001; **Revised** February 18, 2002)

ting diesel spray (Senda et al., 1997). The TAB model of a non-evaporating diesel spray with $\Phi=6$ and $K=0.89$ agreed well with the experimental results. The Φ and K values of the improved TAB model in this study are, respectively, 6 and 0.89, as in previous the non-evaporating spray. Furthermore, the DVM was used to analyze the inner structure of a diesel spray. The concept of liquid length by Siebers and Higgins (Siebers, 1998, 1999) was introduced for switching betaceen TAB model and DVM. Here the simulation process is divided into three steps. The first step analyzes the breakup of a droplet of an injected fuel by using KIVA-II (TAB model). The second step based on the theory of Siebers' liquid length analyzes spray evaporation and switching of the TAB model and the DVM. The final process of DVM calculation reproduces the ambient gas flow and vortex flow of the inner spray with entrainment of ambient gas. A schematic concept of the hybrid model is shown in Fig. 1.

Numerous studies have been conducted on the structure of a spray by DVM (Kamimoto et al., 1993; Kosaka et al., 1995). However, the previous researchers neglected the liquid phase of injected fuel and considered only the vapor phase. They applied the DVM to analyze the spray at the end of evaporation of the injected fuel. However, the information about the liquid phase is also crucial in the spray analysis. Therefore, this study attempts to supplement the overall spray analysis by incorporating the flow analysis of liquid phase before the end of evaporation of the injected fuel Calculation of the liquid phase length based on

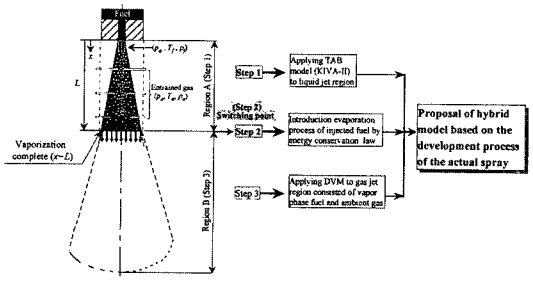

Fig. 1 Hypothesized spray structure with two-regions for simulation

the concept of Siebers. is introduced. Furthermore, the vortex structure of inner spray that could not be captured by experimental measurement using exciplex fluorescence method and by KIVA-II simulation analysis could be obtained by the DVM. The data from the hybrid model were compared with those from the experimental analysis of a free evaporating fuel spray at its early injection stage under in-cylinder like conditions. The exciplex fluorescence method was used to visualize the experimental phenomenon and to simultaneously measure the vapor and liquid phases of the evaporating fuel. To verify validity of the hybrid model, the results obtained by using the hybrid model were also compared with the experimental results.

2. Reviews on Applied Simulation Models

2.1 DVM (Discrete Vortex Method)

DVM based on the Lagrangian analysis is a flow analysis method for the motion of each free vortex, which replaces the continuous distribution of vorticity, which occurs in a flow having different viscosity and density with discrete distribution of free vortex. Previous studies applied the DVM method, which was first proposed by Rosenhead (1931), mainly to separation flow and gas jets with a comparatively high Reynolds number (Shmizu, 1985). The DVM is simple to implement and effective in modeling the essence of vortex formation, and fit for coupling with models that describe the interaction between particles and fluid, because both drop-phase and gas-phase are solved in Lagrangian form. By using DVM, this study deals with the gas jet flow of a two-dimensional unsteady flow based on the assumption of incompressible fluid. In the DVM, the representative model considering viscosity is the Random Walk Method (Chorin, 1973) and vortex core model (Sakata et al., 1983). The vortex core model was used in this study. In the case of inviscid vortex, there is no vorticity diffusion ; however, in the case of viscosity vortex, the temporal diffusion of vorticity should be considered.

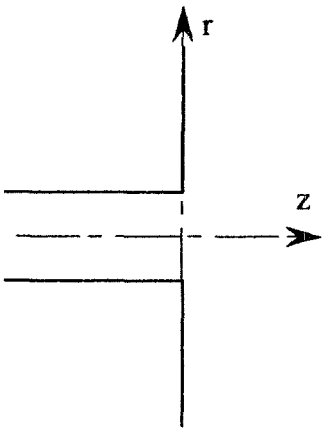

Fig. 2 Coordinate system of flow field (DVM)

Figure 2 shows coordinate system for DVM calculation.

As for the solution to the two-dimensional Navier-Stokes equation as it relates to the viscosity vortex, the vorticity distribution of time T and radius r_v from center can be obtained from the following equation (Nagano Sakata et al., 1981).

$$\omega(r_v,\ T)=\frac{\Gamma}{4\pi vt}\exp\left(-\frac{r_v Re}{4T}\right) \tag{1}$$

Where ω is the vorticity, which is the circulation of a discrete vortex, and r_v is the radial distance from the vortex center, respectively. Also, for vorticity diffusion, the induced velocity can be expressed as the following equation.

$$\begin{aligned} u(T)&=\frac{\Gamma(r_0-r)}{2\pi R^2}\left\{1-\exp\left(\frac{r_v^2 Re}{4T}\right)\right\}\\ v(T)&=-\frac{\Gamma(z_0-z)}{2\pi R^2}\left\{1-\exp\left(-\frac{r_v^2 Re}{4T}\right)\right\}\end{aligned} \tag{2}$$

Where u is velocity component in z-axis direction and v is the velocity component in r-axis direction. The velocities, $u(T)$ and $v(T)$, are equal to 0 at the vortex center. With increasing radius r_v, the velocities also increase and each become maximum value at a position σ'. The position σ' increases with time. The case where the vortex is concentrated on one point at $T=0$ can be explained by the following equation.

$$\sigma'=2.242(T/Re)^{0.5} \tag{3}$$

In Eq. (3), assuming that σ' is vortex core radius and vorticity is constant in the vortex core, the above Eqs. (1) and (2) can be expressed as by equations (4) and (5) below.

$$\omega=\begin{Bmatrix}\dfrac{\Gamma}{\pi\sigma'} & (r_v\le\sigma')\\ 0 & (r_v>\sigma')\end{Bmatrix} \tag{4}$$

$$\begin{aligned} u&=\frac{\Gamma(r_0-r)}{2\pi\sigma'},\ v=-\frac{\Gamma(z_0-z)}{2\pi\sigma'^2} \quad (r_v\le\sigma')\\ u&=\frac{\Gamma(r_0-r)}{2\pi R^2},\ v=-\frac{\Gamma(z_0-z)}{2\pi R^2} \quad (r_v>\sigma')\end{aligned} \tag{5}$$

2.1.1 The attenuation of circulation

In actual flows, even if the mean velocity distribution is two-dimensional, turbulence is, in principle, three-dimensional. The result that describes an actual phenomenon could be obtained by introducing a model that considers the attenuation of circulation (Kiya, et al, 1982). Accordingly, we need to take into account the attenuation of circulation intensity caused by the dissipation of three-dimensional turbulence. In this study, a model represented by Eq. (6) was employed; the equation is the solution of Navier-Stokes equation for the single liner viscous vortex.

$$\Gamma(T)/\Gamma_0=1-\exp(-C/T) \tag{6}$$

Where Γ is the initial circulation intensity and C is constant of circulation attenuation and equal to 30 (Yamane et al., 1994).

2.2 Analysis of liquid phase length for switching both the TAB model and DVM model

In order to investigate the liquid phase length, three non-dimensional groups from Siebers' analysis (Siebers et al., 1999) of liquid-phase length were used. These groups correspond to a momentum scale, an energy scale, and a length scale, respectively. Considering the conservation of mass and momentum, the liquid phase length should be a function of the ratio of the fuel density (ρ_f) to the in-cylinder gas density (ρ_a). In this study, the non-dimensional constant A can be obtained from Eq. (7), which yielded 26. 4 using the Thermophysical Properties of Hydrocarbon Mixture Database (*i.e.*, "NIST program"), (Ely et al., 1992).

$$A=\frac{\rho_f}{\rho_a} \tag{7}$$

Also, the heat transfer from the ambient gas to injected fuel is considered, and the parameter for this is denoted as the "specific energy ratio," which is defined as follows:

$$B=\frac{C_{p,liq}(T_b-T_f)+h_{vap}}{C_{p,air}(T_{air}-T_b)} \tag{8}$$

The fuel properties that are used to obtain the specific energy ratio are as follows: C_p, the specific heat at constant pressure; T_b, the boiling point temperature; T_f, the initial temperature; and h_{vap}, the latent heat of vaporization. T_a is the temperature of the in-cylinder gases. Also, according to Ely et al., (1992) the values of $C_{p,liq}$ and $C_{p,air}$ are 4.48 and 1.11kJ/kgK, respectively. The value of h_{vap} is determined by the estimate method (Ohe, 1985) and equal to 57.53kJ/kg, here. Finally, a length scale for fuel properties from the results of Siebers et al., (1999) can be expressed:

$$\ln\left(\frac{x_{liq}}{d_0}\right)=\ln k'+\alpha \ln A+\beta \ln B \tag{9}$$

where according to the results of Siebers et al. (1999), the k', α, and β are constants whose value are, 10.5, 0.58, and 0.59, respectively. Using this equation, the liquid length x_{liq} calculated to 36mm for the experimental condition of this study.

3. Experimental Apparatus and Procedure

3.1 Experimental apparatus

Figure 3 shows a schematic diagram of the experimental apparatus. The experiments were conducted inside a constant volume, high pressure vessel, which was maintained its ambient temperature and back pressure, at 700K and 2. 55MPa respectively. This vessel consists of two quartz glass windows, which were installed perpendicular to each other. Thus, the fluorescence emissions from the spray irradiated with a laser light sheet could be measured. Nitrogen was utilized as the ambient gas to prevent quenching

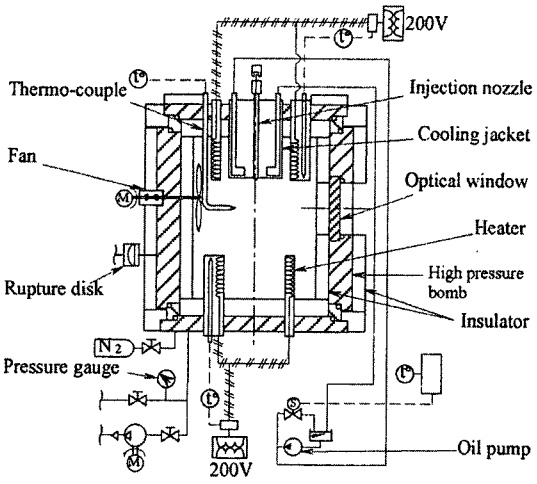

Fig. 3 Experimental apparatus

of liquid phase fluorescence by oxygen. This ambient gas was heated using heaters inside the vessel.

3.2 Experimental and simulation conditions

3.2.1 Experimental condition

The n-tridecane as the reference fuel oil of JIS second class gas oil was injected into the quiescent atmosphere of nitrogen gas through a single hole injector. Naphthalene of 9% mass and TMPD (N, N, N', N' tetramethyl-p-phenylene diamine) of 1% mass were mixed in n-tridecane to obtain the fluorescent emissions of vapor and liquid phases. The TMPD was mixed with *n*-tridecane in nitrogen atmosphere to prevent the oxidation of TMPD. The high pressure injection system (ECD-U2 system) developed by Denso Co., Ltd. was used. The diameter and the length of nozzle were 0.2mm and 1.0mm, respectively. The ambient gas density and ambient gas temperature were 12.3kg/m^3 and 700K, respectively. The injection pressure and the fuel injection quantity were kept constant at 72MPa and 12mg, respectively.

Table 1 shows the summary of experimental conditions.

Figure 4 is a schematic diagram of the optical system used in this study. The light source was the third harmonic of an Nd:YAG laser at 355nm

Table 1 Experimental conditions

Injection nozzle	Type : Hole nozzle DLL-p	
	Diameter of hole d_n [mm]	0.2
	Length of hole L_n [mm]	1.0
Ambient gas		N_2 gas
Ambient temperature	T_a [K]	700
Ambient pressure	p_a [MPa]	2.55
Ambient density	ρ_a [kg/m^3]	12.3
Injection pressure	p_{inj} [MPa]	72
Injection quantity	Q_{inj} [mg]	12.0
Injection duration	t_{inj}	1.54

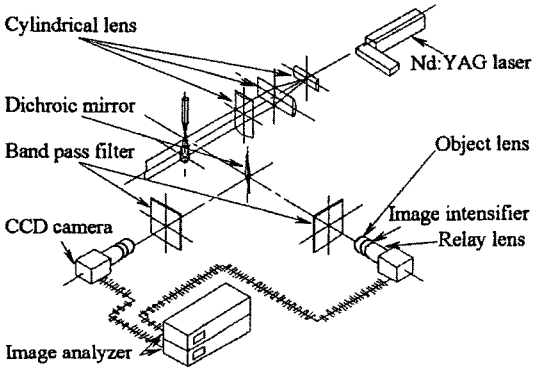

Fig. 4 Schematic diagram of laser sheet optical system and photography system

(power 60mJ/pulse, pulse width : 8ns., maximum frequency : 10Hz, beam diameter : 6.4mm, beam shape : doughnut type). A thin sheet of laser light formed as the light passed through three sets of cylindrical lenses made of quartz. The width and the thickness of the light were 50mm and 0.2mm, respectively. The lenses have high transmissivity in the ultraviolet region by essence of their material, and they were given non-reflective coating; consequently, the energy of laser light hardly damped. Then a thin sheet of laser light was coming to the section of a free diesel spray and the fluorescence emissions from both vapor and liquid phase were generated. The spectra of fluorescence emissions from both phases were separated by a dichroic mirror system and two sets of band pass filters. The dichroic mirror, a blue reflection type, had a 470nm wavelength of 50% refection. The center wavelengths of the band

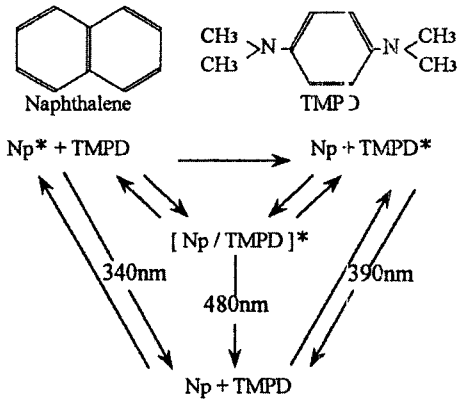

Fig. 5 Schematic summary of naphthalene and TMPD exciplex system

pass filter for vapor and liquid phases widths were 390nm and 532nm and their half widths were 19nm and 2nm, respectively. In the exciplex fluorescent system of naphthalene and TMPD, the exciplex corresponding to the information of the liquid phase generates its fluorescence at 480nm. However, the selected wavelength of the liquid phase was different from this wavelength, which accounts for the stronger fluorescent intensity from this phase than that from the vapor phase (Senda et al., 1996). The emissions from both phases were increased in their luminosity by the image intensifiers after they came through the objective lenses. Thereafter, intensified emissions are transferred into the relay lenses and are taken by the CCD cameras (number of pixels : 540×480, S/N : 50dB). The photographing speed of CCD camera is 1/30μs. and the lifetime of fluorescent emissions of TMPD and exciplex range from 1ns. to 10^3ns. This experiment was carried out in a perfect photo darkroom. Consequently, the frozen image at the incidence of the laser light could be caught by the CCD camera. The spatial resolution was about 0.1mm/pixel. The signals from images of both phases were transferred into image analyzers and were processed by the A/D conversion (resolution : 8 bits) to obtain the image of 256 gradation.

In the Fig. 5, a schematic summary of the photophysics of the naphthalene/TMPD exciplex fluorescence system proposed by Melton, 1983 and Melton et al. (1984) is shown.

3.2.2 Simulation conditions

3.2.2.1 KIVA-II code (Including improved TAB model)

The results calculated by KIVA-II code with the TAB model were compared with the experimental results. The profiles of the size distribution changed, *i.e.* the degree of freedom Φ of the χ-squared function. The distorting motion of particles was discussed in terms of its energy ratio, *i.e.* the parameter K of the TAB method. This study, like the non-evaporating spray (Senda et al., 1997), tunes the parameters Φ and K for each case of $\Phi=2$, $K=10/3$ and $\Phi=6$, $K=0.89$, respectively. In each case, the distribution function $f(r)$, the weight distribution function $g(r)$ and the cumulative distribution function $h(r)$ are expressed by the following equations.

[Case of $\Phi=2$]

$$f(r)=\frac{1}{\bar{r}}\exp\left[-\frac{r}{\bar{r}}\right] \tag{10}$$

$$g(r)=\frac{r^3}{6\bar{r}^4}\exp\left[-\frac{r}{\bar{r}}\right] \tag{11}$$

$$h(r)=\int_0^r g(r)\,dr$$
$$=1-\left[1+\frac{r}{\bar{r}}+\frac{1}{2}\left(\frac{r}{\bar{r}}\right)^2+\frac{1}{6}\left(\frac{r}{\bar{r}}\right)^3\right]\times\exp\left[-\frac{r}{\bar{r}}\right],\ r\le\frac{r}{\bar{r}}\le 12 \tag{12}$$

[Case of $\Phi=6$]

$$f(r)=\frac{r^2}{6\bar{r}^3}\exp\left[-\frac{r}{\bar{r}}\right] \tag{13}$$

$$g(r)=\frac{r^5}{120\bar{r}^6}\exp\left[-\frac{r}{\bar{r}}\right] \tag{14}$$

$$h(r)=\int_0^r g(r)\,dr$$
$$=1-\left[1+\frac{r}{\bar{r}}+\frac{1}{2}\left(\frac{r}{\bar{r}}\right)^2+\frac{1}{6}\left(\frac{r}{\bar{r}}\right)^3+\frac{1}{24}\left(\frac{r}{\bar{r}}\right)^4+\frac{1}{120}\left(\frac{r}{\bar{r}}\right)^5\right]\times\exp\left[-\frac{r}{\bar{r}}\right],\ r\le\frac{r}{\bar{r}}\le 21 \tag{15}$$

Where r is the particle radius and $\bar{r}$ is the arithmetic average radius of the particles. For each distribution function $f(r)$, $\bar{r}$ is related to the input *Sauter* mean radius r_{32}, $\bar{r}=r_{32}/3$ [for Eq. (10)] and $\bar{r}=3r_{32}/5$ [for Eq. (13)]. In the TAB method (O'rourke et al., 1987), the motion of a particle is described with conservation of its energy before breakup E_{old} and after breakup E_{new}. The equations for E_{old} and E_{new} are given by the following.

$$E_{old}=4\pi r^2\sigma+K\frac{\pi}{5}\rho_d r^5(\dot{y}+\omega'^2y^2) \tag{16}$$

$$E_{new}=4\pi r^2\sigma\frac{r}{r_{32}}+\frac{\pi}{6}\rho_d r^5\dot{y} \tag{17}$$

Where, r is the particle radius before breakup and r_{32} is the Sauter mean radius after breakup, and σ is the surface tension of particle, and ρ_d is particle density, and y is the non-dimensional displacement of the particle surface and ω' is the oscillation frequency. K is the ratio of the distorting energy of particle to its total energy. Assuming conservation of energy in particle motion with $y=1$ in oscillation and breakup, the following equation can be obtained from setting Eq. (16) =Eq. (17).

$$r_{32}=\frac{r}{\left[1+\frac{8K}{20}+\frac{6K-5}{120}\left(\frac{\rho_d r^3}{\sigma}\right)\dot{y}^2\right]} \tag{18}$$

The energy ratio K is determined as $K=10/3$ in the original TAB model (O'rourke et al., 1987).

Figure 6 shows the spray tip penetration versus time for the various Φ and K. As shown this

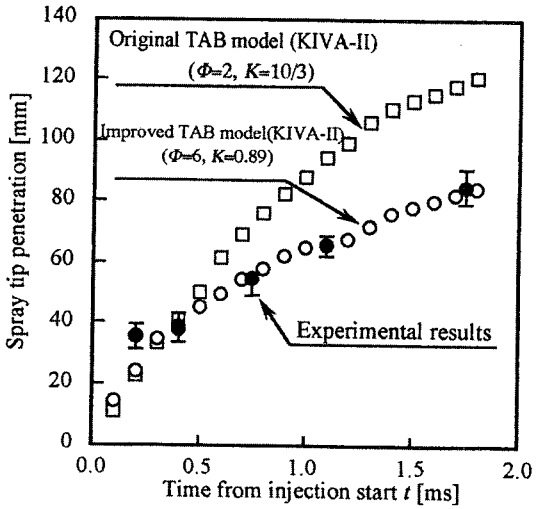

Fig. 6 Temporal change in spray tip penetration for calculational and experimental results

Table 2 Computational conditions (KIVA-II code)

Injection velocity	V_{inj} [m/s]	338
Injection duration	t_{inj} [ms]	1.54
Injection quantity	Q_{inj} [mg]	12.0
Initial droplet temperature	T_{pi}[K]	293
Fuel		*n*-Tridecane
Number of parcel	N_p	1000
Ambient temperature	T_a [K]	700
Ambient density	ρ_a [kg/m^3]	12.3
Maximum time step	dt_{max} [s]	1.0×10^{-6}
Minimum tims step	dt_{min} [s]	0.5×10^{-8}
Number of mesh		23×1×70 (sector mesh)

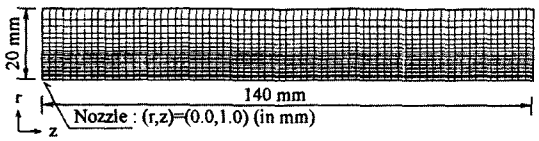

Fig. 7 Computational mesh

figure, it can be concluded that the cases of $\Phi=6$ and $K=0.89$ could successfully estimate the actual droplets distribution and spray tip penetration in the diesel spray.

Table 2 shows calculation condition used in this study. The used fuel is also n-tridecane (as in experimental case). The injection pressure and density of ambient gas are $p_{inj}=72$ MPa and $\rho_a=12.3$kg/m^3, respectively, as shown in Table 2. These values correspond with those in the experiment as mentioned above. Computations using both the original KIVA-II (TAB) model and the improved model were executed in an axial symmetry of 2-dimensional assumption with the sector mesh (central angle 0.5deg.) as shown in Fig. 7.

The ambient field was set in the radial direction at $r=20$mm with 23 meshes and in the axial direction at $z=140$mm with 70 meshes. Toward the radial direction, the length of each mesh Δr was 0.5mm between $r=0.0$mm and $r=8.0$mm, as stated in literature (Kikuta et al., 1992). The lengths of meshes were constant at $\Delta z=2.0$mm toward the axial direction. A single hole nozzle was located at $(r, z)=(0.0, 1.0)$ (in [mm]), and the parcels were injected toward the z direction.

The TAB method and the standard k-ε turbulent model were used for all calculations in this study. Other parameters in the TAB method were kept constant, namely, $amp0=0.0$, $C_k=8$, $C_d=5$, and $C_F=1/3$.

3.2.2.2 DVM model

The calculation condition of DVM is the same as that of KIVA-II code. Since the DVM is to simulate a turbulent gas jet, the DVM needs to set the gas velocity U_0m/s, the diameter of gas jet Hmm, and kinematic viscosity of ambient gas $\nu_g$mm^2/s as the initial conditions. In this study, the values of these parameters were obtained from the results of Dan et al. (1997) which are based on the conservation of the momentum of the non-evaporating diesel spray. The DVM mechanism is related to the concept of droplet diffusion by Kosaka et al. (1995). The momentum between the diesel spray and the gas jet is related as follows.

$$H\cdot U_0=(\rho_l/\rho_g)^{1/2}\cdot d_n\cdot u_{inj} \tag{19}$$

Where ρ_l is the liquid density, and d_n is the nozzle hole diameter, and u_{inj} is the injection velocity of liquid at the nozzle exit and ρ_g is the gas density. Here, the evaporated gas consists of the nitrogen of ambient gas and n-tridecane of used fuel (mole fraction N_2:$C_{13}H_{28}=0.96$:0.04) in the middle region of $Z=35\sim65$mm from nozzle exit. The mole fraction can be calculated by the mean fluorescence intensity and quantification scheme of vapor phase concentration from exper-

Table 3 Computational conditions (Discrete Vortex Method)

Nozzle hole diameter	H [mm]	11
Issue velocity	U_0 [m/s]	64.2
Gas (mole fraction)		n-Tridecane (0.04), N_2 (0.96)
Gas density	ρ_g[kg/m^3]	14.5
Gas kinematic viscosity	ν_g [mm^2/s]	1.99
Reynolds number at nozzle		355,000
Injection duration	T	10.0(1.71[ms])
Time step	ΔT	0.025

imental results of exciplex fluorescence method. The density (ρ_g) of gas having such a mole fraction is 14.5kg/m^3 at T_a=700K and p_a= 2.55MPa using the NIST program. Furthermore, the equivalent diameter of the gas jet, H=11mm, is the width of spray at the distance from nozzle exit, Z=38mm, that is, based on the concept of Siebers et al. (1999). In our experimental results, H=11mm is used as one of the initial condition in DVM simulation. Hence, the Eq. (19) can be calculated by determining an unknown, U_0. However, in the calculation for U_0, H is 6.8mm, which is the value of spray width of liquid phase at Z=38mm, because the velocity of liquid phase dominates the spray development in the axial direction. H=6.8mm is only used when calculating U_0. As a result, the gas jet velocity was determined to be U_0=64.2m/s by using H= 6.8mm. The gas jet can be assumed to inject with velocity U_0=64.2m/s from nozzle diameter, H= 11mm. The kinematic viscosity of ambient gas ν_g is equal to 1.99mm^2/s by the NIST program.

Table 3 shows the summary of the calculation conditions for DVM. For the calculation, a non-dimensional time T was employed, and the time T was derived from $t(U_0/H)$. The time step ΔT corresponded to time interval of vortex shedding, which is equal to 0.025.

4. Results and Discussion

4.1 Results on experiment of exciplex fluorescence method

Figure 8 shows the two-dimensional fluorescence intensity images of the free spray with injection pressure change obtained by exciplex fluorescence method. In the figures, the (i), (ii) are the vapor and liquid phase of the injected fuel, respectively. The photographing timing was set when the injected fuel mass was almost the same in the each injection pressure, that is, when t/t_{inj} was almost equal at each injection pressure. In the each figure, the liquid phase is wider than the vapor phase in the upper region of the spray, because photographing the vapor phase, a large aperture was selected in order to reduce the halation region due to the TMPD monomer fluorescence of liquid phase. On the other hand, when photographing the liquid phase, the small aperture was selected in the optical system to capture the liquid phase region of low concentration. Consequently, the liquid phase image is larger than the vapor phase image. In the Fig. 8, the low vapor luminance of the upstream spray spreads in the radial direction. With increasing injection pressure, the atomization and evaporation of the diesel spray were promoted by the increase of shear force caused by the interaction between the injected fuel and ambient gas. The fluorescence intensity of the liquid phase rapidly decreases in the vicinity of Z=40mm from the nozzle tip. Also, in each condition of injection pressure, the meandering flow of the mainstream region starts on the spray radial direction at the distance of Z=40mm. As a result, it could be speculated that the transition point at which the momentum of the spray interchanges with the ambient gas is, approximately, in the vicinity of Z=40mm. Consequently, the vortex flow of the ambient gas dominates spray development in the

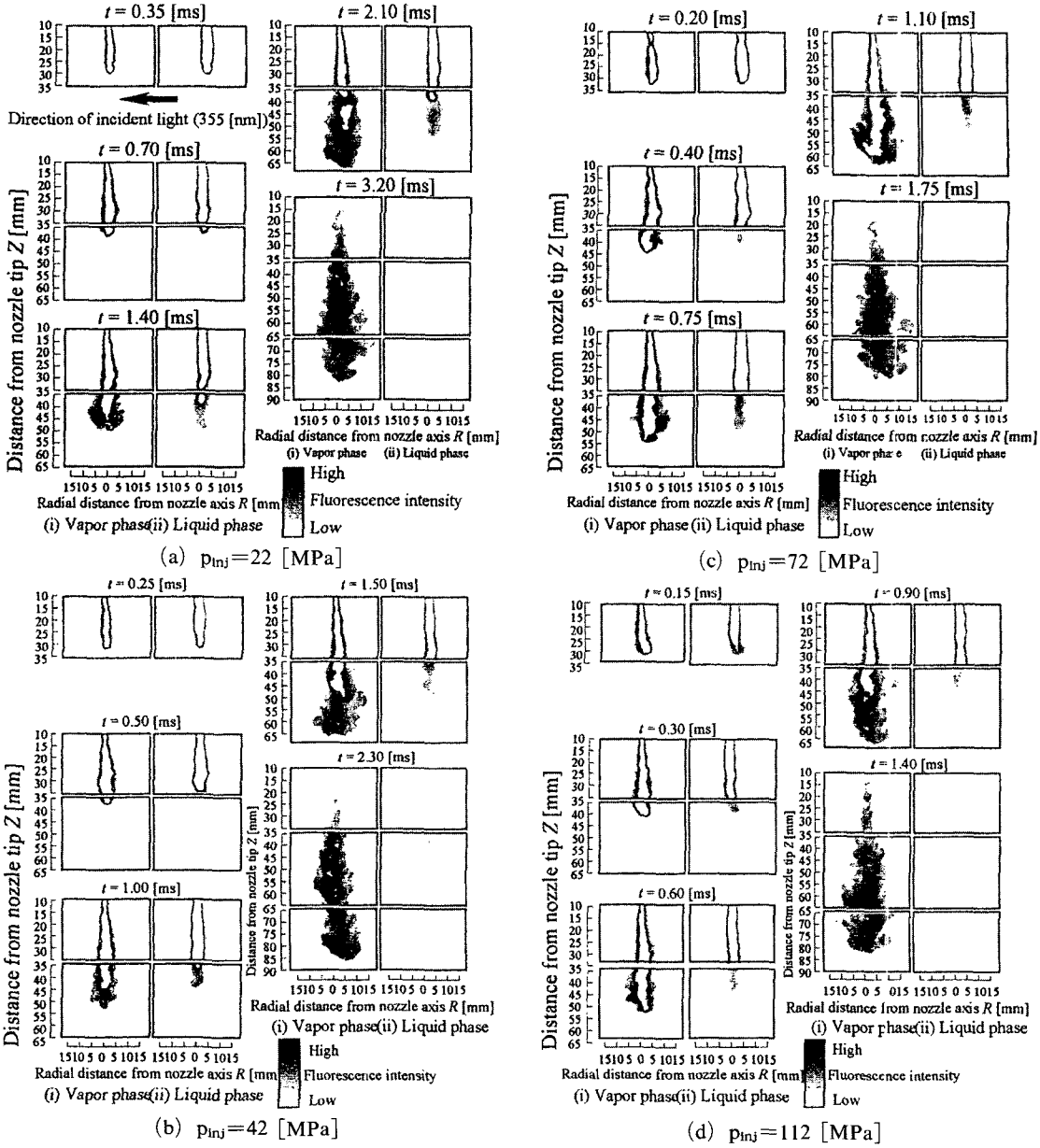

Fig. 8 Temporal change in free spray image with exciplex fluorescence method (Q_{inj}=12.0[mg], ρ_a=12.3[kg/m^3], T_a=700[K]

latter part of the injection.

Figure 9 shows the temporal change in spray tip penetration of the vapor and liquid phase. In the figure, the horizontal axis is the non-dimensional time from the start of injection with each injection duration. The spray tip penetration of liquid phase l_{liq} is determined by the overall fluorescence intensity region in the images. Then, the penetrations at each injection pressure is compared with the same mass of injected fuel, because the profile of the injection rate with time is almost rectangular in this study. The spray tip penetrations of the vapor and the liquid phase were plotted in the same curve as shown in Fig. 9. Consequently, they are independent of injection pressure in non-dimensional time. As a result,

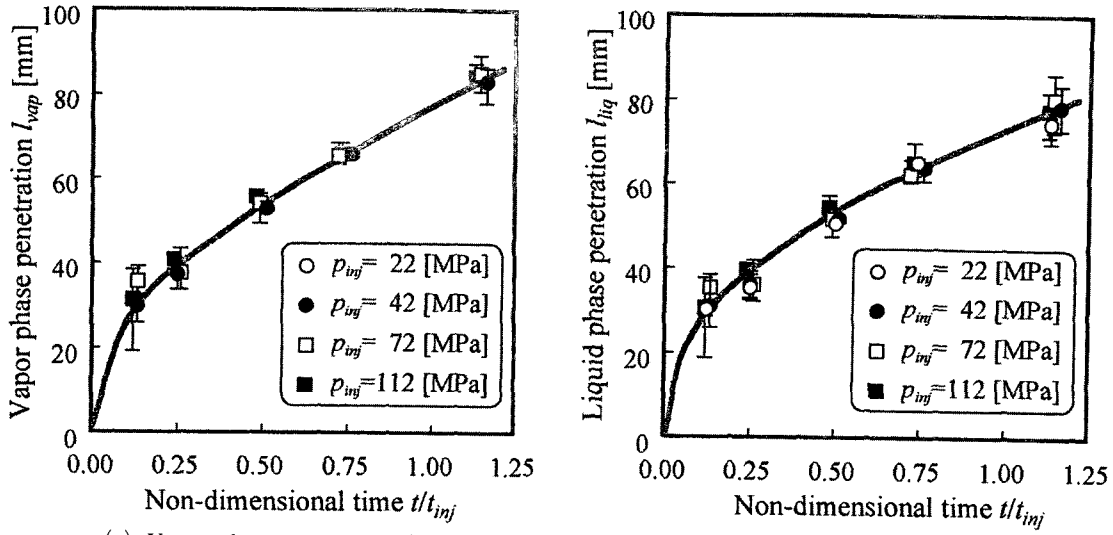

(a) Vapor phase penetration l_{vap} (b) Liquid phase penetration l_{liq}

Fig. 9 Temporal change in penetration of vapor and liquid phase (parameter : injection pressure)

with the same mass of fuel in the injected spray, the spray tip penetration does not depend on injection pressure, the same as a non-reaction diesel spray (Dan et al., 1996). As shown in Fig. 9, the penetration of liquid and vapor phase increase with elapsing time. However, a convergence tendency of the liquid phase length value, as shown in the other experiments using evaporative spray (Espey et al., 1994, 1995, 1997; Hodges et al., 1991; Baritaud et al., 1994), could not be observed. Hence, we conducted tuning for images of liquid phase.

Figure 10 shows the liquid phase length L_{liq} versus the elapsing non-dimensional time. In this study, the liquid phase length L_{liq} is defined by the spatial region where fluorescence intensity marked by 255 gradation of the spray's center decreases to 10% (230~255) of it value in each image. As shown in Fig. 10, the value of the liquid phase length is almost 38 mm in the curve. As a result, the liquid phase length as measured in Fig. 10 is equal to the liquid phase lengths of experiments (Espey et al., 1994, 1995, 1997; Hodges et al., 1991; Baritaud et al., 1994). Moreover, the behavior tendency of liquid phase was found to change at the start point of spray development in the radial direction as shown in

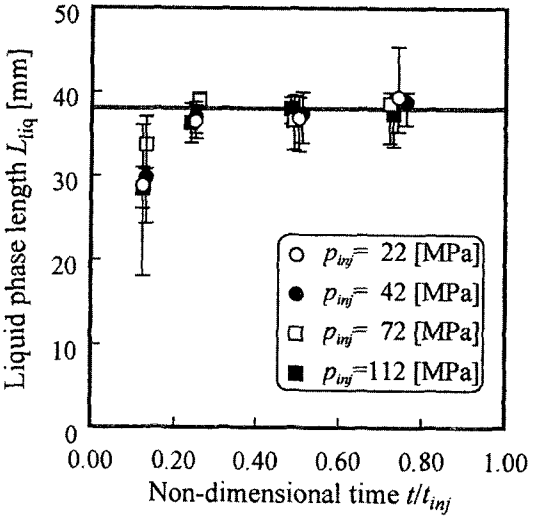

Fig. 10 Temporal change in liquid phase length

Fig. 8. This means that the distance of 38mm from nozzle exit corresponds to the end of momentum exchange from the liquid jet to the ambient gas in non-evaporating spray (Dan et al., 1997).

4.2 Results with the use of the improved TAB model

Figure 11 shows the calculation results with the improved TAB model. In this figure, (a) is the vapor concentration of the injected fuel, and (b)

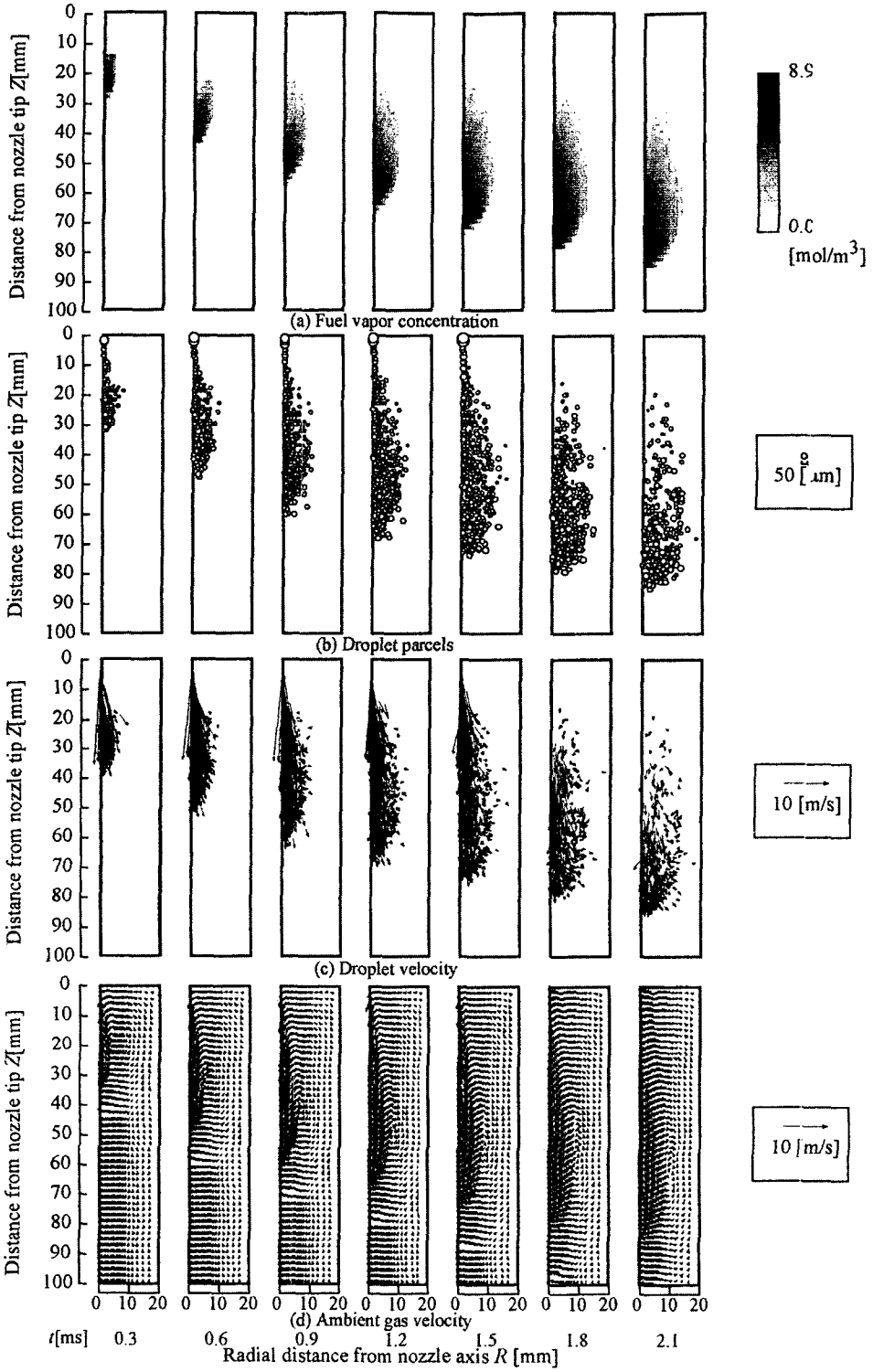

Fig. 11 Temporal change in spatial distribution of fuel vapor concentration, droplet parcels, droplet velocity, and ambient gas velocity with improved TAB model (p_{inj}=72 [MPa], t_{inj}=1.54 [ms], ρ_a=12.3 [kg/m^3]

is spatial distribution of droplets, and (c) is velocity distribution of droplet, and (d) is spatial distribution of ambient gas velocity. In the Figs. 11(a) of calculation results, the formation of vapor phase such as Fig. 8 which is generated by the shear-force between injected fuel and ambient gas near the nozzle was not found. The above result was caused by the TAB breakup model which is a submodel of the KIVA-II code in calculation of droplet breakup. The TAB breakup model is based on oscillation and distortion of droplets. Thus, there are no the atomized droplets and the formation of vapor phase caused by shear-force in the vicinity of the nozzle, and the droplets are larger near the nozzle. Furthermore, as for a remarkable difference between the calculation results and the experimental results, it can be enumerated that the distribution of droplet parcels spreads widely in the radial direction and the high concentration region of vapor fuel is in the region of the spray tip. As a result, the use of the droplet evaporation model in this study should be promoted because the amount of droplet evaporation is underestimated.

Figure 12 shows the change in tip penetration of injected liquid and vapor spray with time. In the Fig. 12, the results from the improved TAB model are in good agreement with the experimental results, and the improved KIVA-II code can successfully reproduce the diesel spray behavior in evaporating field. Furthermore, the calculation results for spray tip penetration of vapor and liquid phase correspond to the experimental results, and also show the possibility that the spray development is dominated by the liquid phase of the injected fuel in the axial direction. Figure 11(c) shows the velocity distribution of droplets. The velocity vector of droplets near the central spray develops along the central axis of the spray. On the other hand, the velocity distribution of the droplets is turbulent in the periphery of the spray because the droplets lost in the momentum are subject to ambient gas flow. As shown in Fig. 11(d), the ambient gas is entrained into the spray and proceeds along the central axis of the spray. Moreover, the entrained ambient gas revolves in the radial direction, with its vertical velocity component in the spray periphery. Then, the spray formation mechanism, like experimental results (Dan et al., 1996) can be also speculated from the results of KIVA-II code, namely, the motion of ambient gas is induced by the fuel injection, and the induced motion related to the flow of droplets and vapor fuel dominates

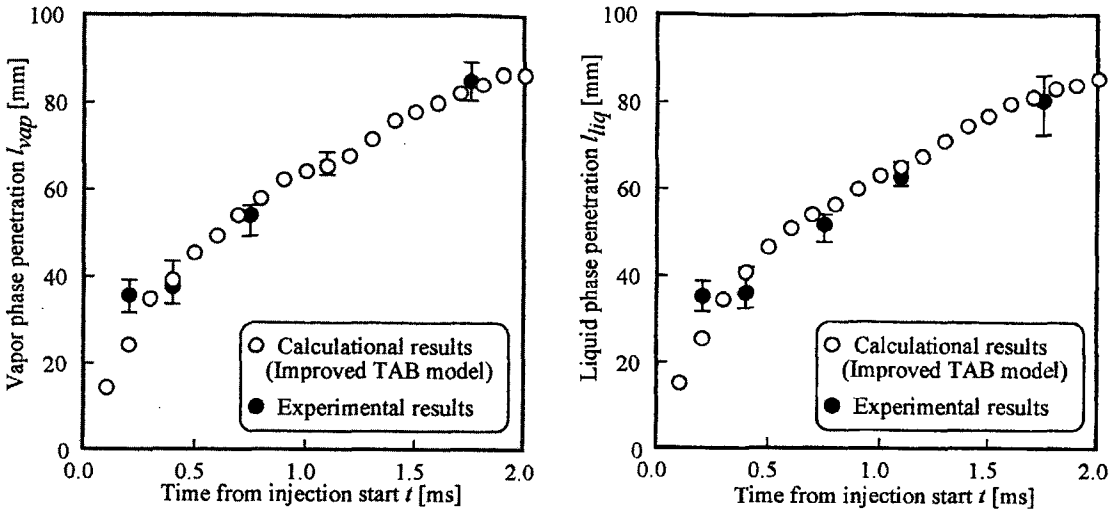

(a) Vapor phase penetration l_{vap} (b) Liquid phase penetration l_{liq}

Fig. 12 Temporal change in penetration of vapor and liquid phase (p_{inj}=72 [Mpa], ρ_a=12.3 [kg/m^3]

the spreading of the spray.

4.3 Results on hybrid model consisted of improved TAB and DVM

Figure 13 shows time change of the droplet parcels distribution in the hybrid model, which consists of the TAB model and distribution of tracers with DVM. As stated, first the improved TAB model ($\Phi=6$ and $K=0.89$) is applied in the hybrid model calculation to the atomization of the liquid jet. Second, the TAB model is switched to the DVM by introducing the liquid phase length, described by Siebers et al., (1999). Third, the DVM is applied to analyze the downstream spray structure and ambient gas flow. In this figure, the distance from virtual origin can be used to measure the real distance from the nozzle exit. The time from the virtual origin time t ms is the real time after injection start. As shown in Fig. 13, in this study, the origin of DVM locates the distance from the virtual origin, 40 mm, where the spray of the liquid jet turns to the gas jet. In the hybrid model, the spatial distance and time for switching the TAB model into the DVM are 40mm and 0.31ms, respectively, based on the concept of Siebers and experimental results of the this study using exciplex fluorescence method. In the Fig. 13, the separated crosswise tracers form the two small vortices at $T=2.5$ (T is the non-dimensional time, $t(U/H)$), and with elapsing time, the tracers with the twin vortices thread proceed downstream at $T=5.0$. The tracers proceeded on central axis are stagnated by the drag force from the ambient gas. The vortex shedding finishes and the profile of meandering near the nozzle can be found. The characteristic tendency of the spray structure corresponds qualitatively to the experimental results.

In Fig. 14, the spray tip penetration is plotted against time from the injection start for the experimental results and the hybrid model. Here, the liquid phase length, $L_{liq}=40$mm is determined by the equations of Siebers ($L_{liq}=36$mm) and experimental results of this study using exciplex fluorescence method ($L_{liq}=38$mm). The time $t_s(=0.31\text{ms})$ is required time for switching to the DVM after calculation of improved TAB model. As shown in Fig. 14, although the results of hybrid model are slightly different from experimental results, the utility of the hybrid model was verified.

Figure 15 shows the temporal change in droplet

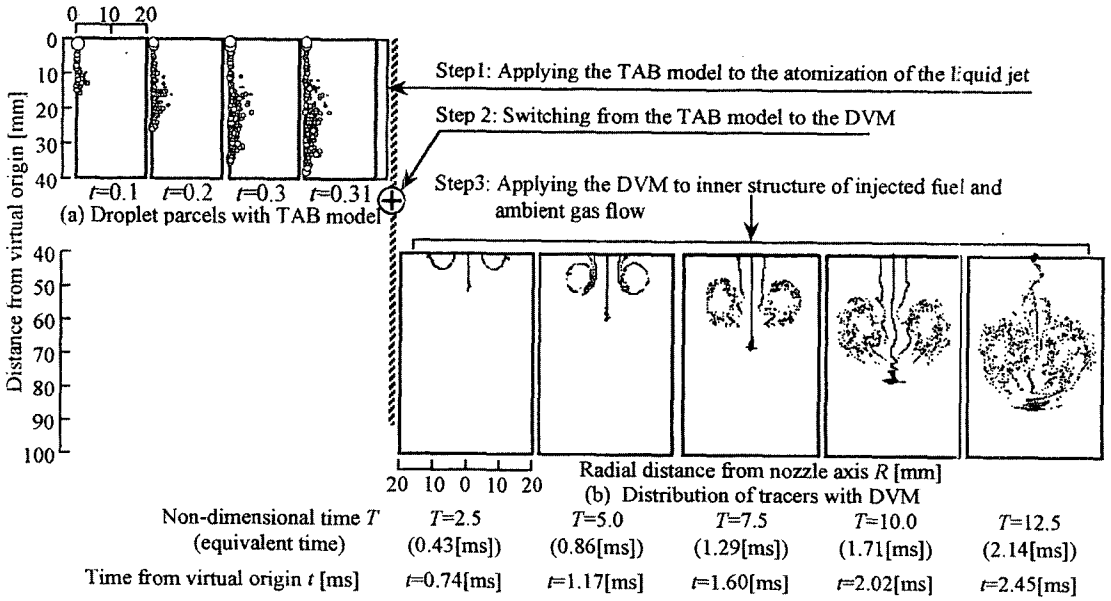

Fig. 13 Temporal change in droplet parcels with TAB model and distribution of tracers with DVM ($H=11$ [mm], $U_0=64.2$ [m/s], $\nu_g=1.99\times10^{-6}$[m^2/s], $Re=3.55\times10^5$, $T_{inj}=10.0$ (1.71 [ms]))

velocity with the use of the TAB model and ambient gas velocity with the use of the DVM.

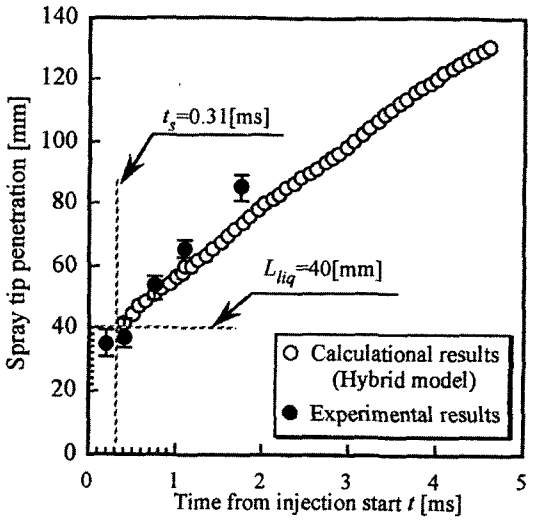

Fig. 14 Temporal change in spray tip penetration for calculation and experiment results

First of all, as shown in Fig. 15(b) [the region of TAB model region (Step 1)], although ambient gas flow occurs slightly in the spray periphery, the entrainment phenomenon of ambient gas cannot be seen in the inner region of the spray. Furthermore, the velocity vectors in the inner region of spray proceed uniformly to the downstream of spray. Hence, it is concluded that there is no entrainment of ambient gas in the region of liquid phase length, and the momentum exchange between injected fuel and ambient gas due to the shear-force mainly occurs at the liquid phase length region of the diesel spray. On the other hand, in the Fig. 15(c) [the region of DVM beyond 40mm from the nozzle exit (Step 3)], the velocity vectors of the ambient gas are rotating in the region of the inner spray due to the momentum exchange in the upper region of the spray. Namely, ambient gas entrains from the region at which the penetration distance of liquid

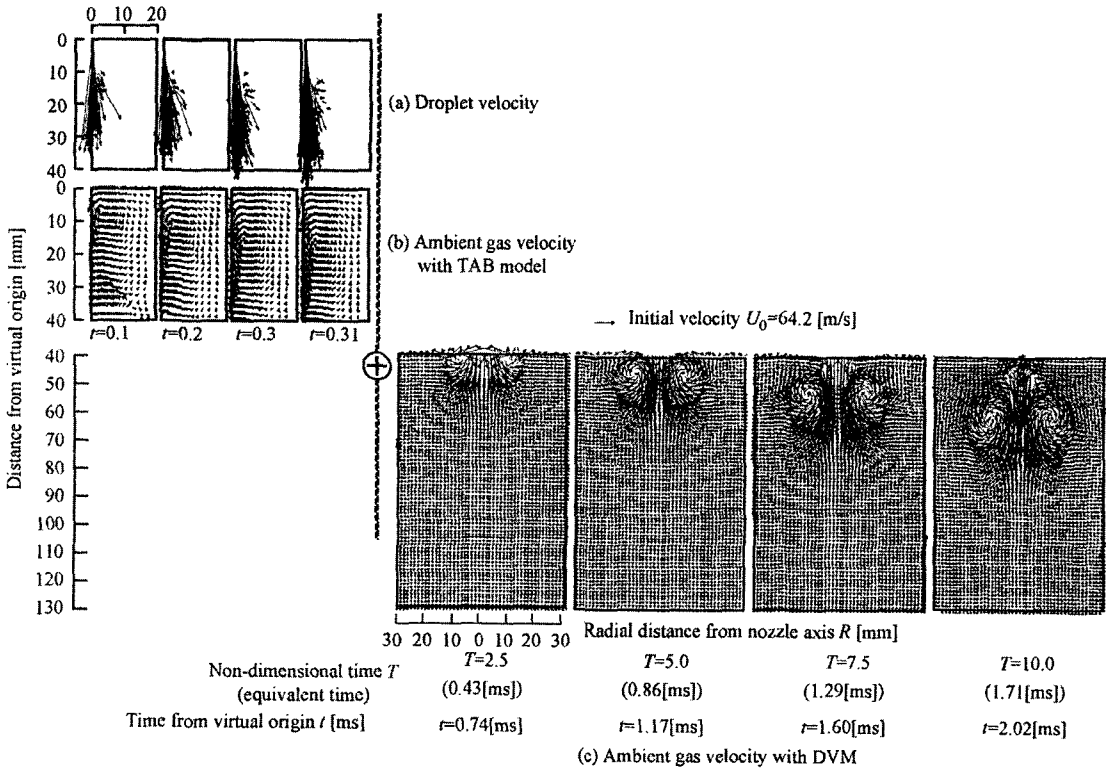

Fig. 15 Temporal change in droplet proplet velocity and ambient gas velocity TAB model and ambient gas velocity with DVM
(H=11 [mm], U_0=64.2 [m/s], ν_g=1.99×10^{-6}[m^2/s], Re=3.55×10^5, T_{inj}=10.0 (1.71 [ms]))

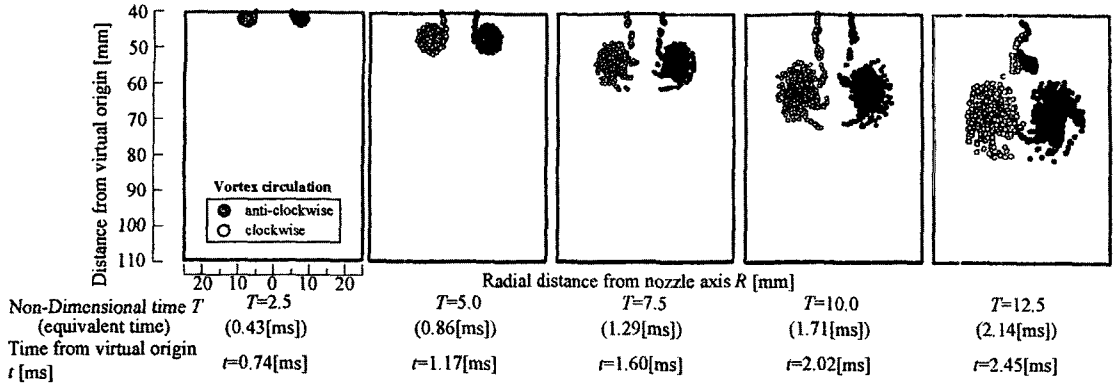

Fig. 16 Temporal change in distribution of vortices

phase fuel is maximum, 40mm. Therefore, the results from the hybrid model sufficiently explain the development process and structural characteristics of the diesel spray in the evaporating field, as Senda et al. (1997) described them for the non-evaporating fuel spray. Furthermore, it can be found that the velocity distribution at each time shows the flow profile of the separated crosswise at the region of the spray tip. The circulations proceed to downstream of gas jet, and the circulation flow gradually becomes larger with time. This figure, like the case of the tracers distribution, shows also the profile of meandering flow after the end of injection.

Figure 16 shows the distribution, circulation direction, and intensity of the vortex-let. As shown in this figure, the vortex-lets concentrate in the same region where turbulent velocity varies, as shown in Fig. 15. Thus, it could be that the vortex-let induces the two vortices thread with crosswise, such as the figure at $T=2.5$ and meandering flow at the end of injection. From the analysis mentioned above, it can be verified that the structure of the gas jet obtained from applying DVM corresponds qualitatively to the structure of evaporating spray from the experimental results. In other words, the structure formation mechanism of the gas jet formed by vortex shedding is equal to that of the evaporating spray formed by a large vortex, induced by the first perturbation (Azetsu et al., 1990) that occur upstream of the spray.

Figure 17 shows the results of penetration for

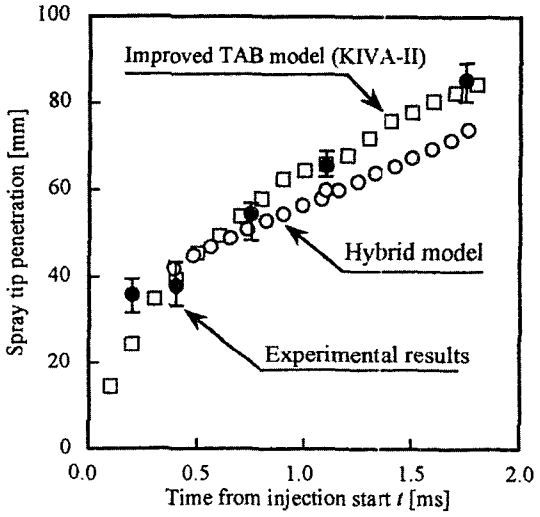

Fig. 17 Temporal change in spray tip penetration for computational and experimental results

the result of experiment, improved TAB model, and hybrid model. The spray tip penetrations in the experiment and the improved TAB model are the measurement results for the vapor phase of the fuel, respectively. In the figure, the simulation method of the improved TAB and the hybrid model can successfully predict the spray tip penetration under the condition of evaporating diesel fuel spray. However, with the improved TAB model, the structure of inner spray and ambient gas flow could not be precisely reproduced. Therefore, the hybrid model proposed in this study is useful to model diesel fuel sprays, properly accounting for the characteristics of spray structure and ambient gas flow.

5. Conclusions

An experiment and simulation were performed for the evaporating fuel spray in this study. In this experiment, the exciplex fluorescence method was used, which can simultaneously measure the vapor and liquid phase of the injected fuel. On the other hand, the simulation was performed using the improved TAB model and hybrid model consisted of the improved TAB model and DVM. In the hybrid model, the improved TAB model was used to compute the atomization of droplets while the DVM was used to analyze turbulent flow of gas jet beyond liquid phase length. The following conclusions are drawn from this study.

(1) The liquid phase length of an evaporating spray converges on a value regardless of the change of injection pressure. In this study, the value is close to 38mm.

(2) The improved TAB model constants of Φ (degree of freedom) $=6$ and K (energy ratio of particle motion) $=0.89$, which were applied to evaporating fuel spray, are sufficiently accurate for analyzing the macro spray structure.

(3) The hybrid model, which consisted of the improved TAB model and DVM, can properly represent the characteristics of vortex flow caused by the entrainment of ambient gas downstream of the diesel spray. The vortex flow in the downstream portion of the evaporating spray evaluated by the DVM showed qualitative agreement with experimental results.

References

Ahmadi-Befrui, B., Uchil, N., Gosman, A. D. and Issa, R., 1996, "Modeling and Simulation of Thin Liquid Films Formed by Spray-Wall Interaction," SAE Paper, No. 960627.

Amsden, A. A., Ramshow, J. D., O'Rourke, P. J. and Dukowiez, J. K., 1985, "KIVA : A Computer Program for Two- and Three-Dimensional Fluid Flows with Chemical Reactions and Fuel Sprays," Los Alamos National Laboratory report LA-10254-MS.

Amsden, A. A., O'Rourke, P. J. and Butler, T. D., 1989, "KIVA-II : A Computer Program for Chemically Reactive Flows and Sprays," Los Alamos National Laboratory report LA-11560-MS.

Amsden, A. A., 1993, "KIVA-3 : A KIVA Program with Block-Structured Mesh for Complex Geometries," Los Alamos National Laboratory report LA-12503-MS.

Amsden, A. A., 1997, "KIVA-3V : A Block-Structured KIVA Program for Engines with Vertical or Canted Valves," Los Alamos National Laboratory report LA-13313-MS.

Azetsu, A., Dodo, S., Someya, T. and Oikawa, C., 1990, "A Study on the Structure of Diesel Spray (2-D Visualization of the Non-Evaporating Spray)," *COMODIA 90* (in Kyoto), pp. 199~204.

Baritaud, T. A., Heinze, T. A. and Le Coz, J. F., 1994, "Spray and Self-Ignition Visualization in a DI Diesel Engine," SAE Paper, No. 940681.

Chorin, A. J., 1973, "Numerical Study of Slightly Viscous Flow," *J. Fluid Mech.*, Vol. 57, Part 4, pp. 785~796.

Dan, T., Takagishi, S., Oishi N., Senda J. and Fujimoto, H., 1996, "The Study of the Spray Structure in the High Injection Pressre" *JSME* 62-597, pp. 2079~2085.

Dan, T., Takagishi, S., Oishi N., Senda J. and Fujimoto, H., 1996, "The Effect of Ambient Density on the Spray Structure," *JSME* 62-599, pp. 2867~20873.

Dan, T., Takagishi, S., Senda, J. and Fujimoto, H., 1997, "Organized Structure and Motion in Diesel Spray," SAE Paper, No. 970641.

Ely, J. F. and Huber, M. L., 1992, "NIST Thermophysical Properties of Hydrocarbon Mixtures Database (SUPERTRAPP) Version 1.0 Users' Guide, National Institute of Standards and Technology".

Espey, C., Dec, J. E., Litzinger, T. A. and Santavicca, D. A., 1994, "Quantitative 2-D Fuel Vapor Concentration Imaging in a Firing D. I. Diesel Engine Using Planar Laser-Induced Rayleigh Scattering," SAE Paper, No. 940682.

Espey, C. and Dec, J. E., 1995, "The Effect of TDC Temperature and Density on the Liquid-Phase Fuel Penetration in a D. I. Diesel Engine," SAE Paper, No. 952456.

Espey, C., Dec, J. E., Litzinger, T. A. and Santavicca, D. A., 1997, "Planar Laser Rayleigh Scattering for Quantitative Vapor-Fuel Imaging in a Diesel Jet," COMBUSTION AND FLAME, 109 : 65-86, pp. 65~86.

Hodges, J. T., Baritaud, T. A. and Heinze, T. A., 1991, "Planar Liquid and Gas Fuel and Droplet Size Visualization in a DI Diesel Engine," SAE Paper, No. 910726.

Kiya, M., Sasaki, K. and Arie, M., 1982, "Discrete-Vortex Simulation of a Turbulent Separation Bubble," *J. Fluid Mech.*, 120, pp. 219~244.

Kikuta, K., Cray, B., Chikahisa, T., Murayama, T. and Martin, J., 1992, "Necessary Mesh Conditions for Accurate KIVA Calculation," *10th Internal Combustion Engine Symposium* (in Japan), pp. 331~336.

Kamimoto, T., Yamane, Y., Kosaka, H. and Kobayashi, H., 1993, "Numerical Simulation of Turbulent Mixing in a Transient Jet," SAE Paper 932657.

Kosaka H., Suzuki, T. and Kamimoto, T., 1995, "Numerical Simulation of Turbulent Dispersion of Fuel Droplets in an Unsteady Spray via Discrete Vortex Method," SAE Paper 952433.

Melton, L. A., 1983, "Spectrally Separated Fluorescence Emissions for Diesel Fuel Droplets and Vapor," Applied Optics, Vol. 22, No. 14, pp. 2224~2226.

Melton, L. A. and Verdieck, J. F., 1984, "Vapor/Liquid Visualization in Fuel Sprays," *20th Sympo. (International) on Combustion/The Combustion Institute*, pp. 1283~1290.

Nagano, S., Naito, M. and Tanaka, H., 1981, "A Numerical Analysis of Two Dimensional Flow Past Rectangular Prisms by a Discrete Vortex Method," *Transactions of JSME (B)*, Vol. 47, No. 413. pp. 32~43.

Ohe, S., 1985, "Estimate Method of Property Constants for Beginner," Nikkan Engineering Paper Corp., pp. 215~221 (in Japanese).

O'Rourke, P. J. and Amsden, A. A., 1987, "The TAB Method for Numerical Calculation of Spray Drop Breakup," SAE Paper, No. 872089.

Rosenhead, L., 1931, "The Formation of Vortices from a Surface of Discontinuity," Proc. R. Soc. Lond., A-134, pp. 170~192.

Sakata, H., Adachi, T. and Inamuro T., 1983, "A Numerical Analysis of Unsteady Separated Flow by Discrete Vortex Model (1st Report, Flow Around a Square Prism)," *Transactions of JSME (B)*, Vol. 49, No. 440, pp. 801-808, (in Japanese).

Senda, J., Kobayashi, M., Iwashita, S. and Fujimoto, H., 1994, "Modeling of Diesel Spray Impinging on a Flat Wall," SAE Paper, No. 941894.

Senda J., Tanabe, Y. and Fujimoto, H., 1996, "Visualization and Quantitative Analysis on Fuel Vapor Concentration in Diesel Spray," Unsteady Combustion (Kluwer Academic Pub.), pp. 283~294.

Senda, J., Kanda, T., Al-Roub, M., Farrell, P. V., Fukami, T. and Fujimoto, H., 1997, "Modeling Spray Impingement Considering Fuel Film Formation on the Wall," SAE Paper, No. 970047.

Senda, J., Dan, T., Takagishi, S., Kanda, T. and Fujimoto, H., 1997, "Spray Characteristics of Non-Reacting Diesel Fuel Spray by Experiments and Simulations with KIVA II Code," Proceedings of ICLASS-'97 (in Seoul), pp. 38~45.

Shimizu, S., 1985, "An Analysis of a Two-Dimensional Jet by the Discrete Vortex Simulation," *Bull. JSME*, B-51-472, pp. 3852~3859.

Siebers, D. L., 1998, "Liquid-Phase Fuel Penetration in Diesel Spray," SAE Paper No. 980809.

Siebers, D. L., Charles, J. and Higgins, B. S., 1999, "Measurements of Fuel Effects on Liquid-Phase Penetration in DI Sprays," SAE Paper No. 1999-01-0519.

Siebers, D. L., 1999, "Scaling Liquid-Phase Fuel Penetration in Diesel Sprays Based on Mixing-Limited Vaporization," SAE Paper No. 1999-01-0528.

Yamane, Y., Kamimoto, T., Kosaka, H. and Kobayashi, H., 1994, "Numerical Simulation of Entrainment of an Unsteady 2-D Turbulent Jet," *Transaction of JSME (B)*, Vol. 60, No. 572, pp. 1457~1462, (in Japanese).